Influence of Primary Coma on the Tightly Focusing Characteristics of Circular Basis Hybrid Order Poincaré Sphere Beams

Sushanta Kumar Pal *, Rakesh Kumar Singh, Paramasivam Senthilkumaran

Posted Date: 22 December 2023

doi: 10.20944/preprints202312.1701.v1

Keywords: Laser beam shaping; Debye-Wolf Integral; High numerical aperture optics; Hybrid order Poincaré sphere; Polarization; Singular optics

Article

Influence of Primary Coma on the Tightly Focusing Characteristics of Circular Basis Hybrid Order Poincaré Sphere Beams

Sushanta Kumar Pal [1,*], Rakesh Kumar Singh [2], and Paramasivam Senthilkumaran [3]

[1] Centre for Optics, Photonics, and Lasers (COPL), Department of Electrical and Computer Engineering, Université Laval, Québec, QC G1V 0A6, Canada
[2] Laboratory of Information Photonics and Optical Metrology, Department of Physics, Indian Institute of Technology (Banaras Hindu University), Varanasi, 221005 Uttar Pradesh, India
[3] Optics and Photonics Centre, Indian Institute of Technology Delhi, Hauz Khas, New Delhi 110016, India
* Correspondence: sushanta1985@gmail.com

Abstract: We study the tight focusing properties of generic bright and dark HyOPS beams in the presence of primary coma. The role of the polarization singularity index and handedness of the polarization of the HyOPS beams on the focused structure has been discussed. Results have been presented for the total intensity, component intensities, and component phase distributions for left-, and right-handed bright and dark star and lemon types singularities. The presence of primary coma distorted the focal plane intensity distributions for both positive and negative index generic C-points. Coma is known to disturb the circular symmetry of the focal plane intensity distribution. Similarly in tight focusing polarization is known to disturb the symmetry. Therefore, a beam with structured and inhomogeneous polarization distribution tightly focused under the influence of coma is a fit case to study. It is found that the presence of primary coma aberration in the focusing system produces a positional shift of the high-intensity peaks and a reduction of the intensity on one side of the center. As the strength of the primary coma increases, the focal plane intensity distributions shift more and more toward the right from the initial position. Unlike the scalar vortex case, in the case of HyOPS beams, the focal plane intensity distribution undergoes rotation, as the helicity of the HyOPS beams is inverted, in addition to shifting. All the component phase distributions are found to be embedded with phase vortices of charge ± 1.

Keywords: laser beam shaping; debye-wolf integral; high numerical aperture optics; hybrid order poincaré sphere; polarization; singular optics

1. Introduction

The focal plane intensity distribution can be modified by pupil function engineering [1–3]. It was shown that suppression of side lobes in the focal field is possible by apodization [4]. To achieve a perfect focal spot, apertured beams in paraxial [5,6] and non-paraxial focusing [7] were tried. Generation of longitudinal component [8] can be achieved by providing spherical curvature to the beam in high numerical aperture (NA) systems. The dominating role played by the polarization in tight focusing using high NA to shape the point spread function (PSF) was later recognized [9]. Polarization engineering, to shape the PSF by using spatially inhomogeneous polarization, due to its increasing number of applications [10–16] has come under scrutiny in recent years. In tight focusing, generation of significant longitudinal polarization component [12,17], realization of smallest focal spot[17], generation of 3D-polarization structures and singularities [18,19], and topological structures [20,21] and optical Möbius stripes[22–25] are possible by polarization engineering.

In pupil function engineering, using phase and polarization degrees of freedom, the focal plane intensity distributions can be tuned. A phase vortex can be used to produce a doughnut intensity distribution, whereas a polarization vortex can be used to produce the smallest focal spot [12,17]. In a practical optical system, the focal plane intensity distributions may deteriorate due to the presence

 doi:10.20944/preprints202312.1701.v1

of various aberrations. Coma is known to disturb the circular symmetry of the focal plane intensity distribution. Similarly in tight focusing, polarization is known to disturb the symmetry. Therefore, a beam with structured and inhomogeneous polarization distribution tightly focused under the influence of coma is a fit case to study. For a monochromatic optical field, the combined effect of aberrations such as astigmatism, coma, spherical aberration, etc. may be responsible for the deterioration of the image quality. To know the effect of individual aberrations on the focal spot each aberration has been studied separately. Tight focusing of generic hybrid order Poincaré sphere (HyOPS) beams in the presence of primary coma was never studied, which we have studied in the current manuscript.

The present work is the first of its kind. We have summarized previously reported works in this paragraph to find out the novel aspect of our work. Recently tight focusing of vector vortex beams in the presence of spherical aberration has been studied [26]. To date, the effect of coma aberration on the tight focusing of HyOPS beams has not been investigated by anyone. This is the first report which examines the influence of primary coma in a tight focusing system. The tight focusing of phase singular beams is studied in refs.[27,28]. In the case of tight focusing of phase singular beams, the intensity rings become lobes in the presence of primary coma. In a tight focusing system, polarization is found to play a critical role, and hence homogenous and spatially varying polarization distributions can not be considered as the same. This work is important in polarization engineering methods using structured HyOPS beams. The effect of primary coma is different for phase and polarization singularities in a tight focusing system.

Polarization singularities are points at which the azimuth (γ) of the polarization ellipse is indeterminate and are characterized by contour integral $\oint \nabla\gamma \cdot dl \neq 0$ around the singularity. The value of the contour integral for a HyOPS beam, also known as C-point singularity, [29–31] is $p\pi$, where p is an integer. The C-point index is $I_C = p/2$. The state of polarization (SOP) distribution for a C-point consists of ellipses and hence a C-point has helicity [32,33]. On the other hand, there are V-point singularities [31,34,35], characterized by Poincaré-Hopf index η in which the contour integral takes value $2\pi\eta$. V-points consist of spatially varying linear SOP distributions. They have no helicity associated with them. A C-point can be bright or dark depending on the intensity distribution at the C-point. Unlike the C-point, the intensity distribution at a V-point is always zero. The neighborhood polarization distribution around a V-point is linear, whereas it is elliptical for a C-point. In terms of orientation angle the C-point index and V-point index are defined as $\frac{1}{2\pi}\oint \nabla\gamma \cdot dl$. The C-point index can take integer and half-integer values, whereas the V-point index can only take integer values. Polarization singularities can be generated by the superposition of two vortex beams with right and left circular polarization. For a bright C-point, one of the interfering beams is a non-vortex plane beam. Polarization singularities are generally identified by constructing the Stokes field $S_{12} = S_1 + iS_2 = |S_{12}|\exp(i\phi_{12})$. The Stokes phase $\phi_{12} = 2\gamma$ and it can be shown that it is the phase difference between left and right-handed components in the circular basis, i.e., $\phi_{12} = \phi_L - \phi_R$. Therefore, phase vortices of S_{12} Stokes field are polarization singularities.

The C-point polarization singularities are also known as circular basis hybrid order Poincaré sphere (HyOPS) beams [36], whereas the V-point singularities are called circular basis higher order Poincaré sphere (HOPS) beams [37]. Unlike the fundamental Poincaré sphere, on a HyOPS (HOPS) the polarization states of a C-point (V-point) singularity can be represented as a point on the surface of the sphere. Some of the recently reported applications of polarization singularities are in optical signal processing[38], optical chirality measurements[39], optical trapping and manipulation [40], optical lattices[41,42], material machining[43], optical skyrmions[44] and structured illumination microscopy[45].

Aberrations are found to affect the structure of the focal plane field distributions of a focusing system. Therefore a systematic study on the effect of aberrations is needed. In this manuscript, we study the tight focusing properties of generic bright and dark HyOPS beams such as star-type and lemon-type C-points of different helicity in the presence of primary comatic aberration. We show that

Preprints (www.preprints.org) | NOT PEER-REVIEWED | Posted: 22 December 2023 doi:10.20944/preprints202312.1701.v1

the strength of comatic aberration, sign, the absolute value of the C-point index (I_C), amplitude, and helicity of the HyOPS beams play an important role in tailoring the focal intensity landscapes.

2. Theory of Tight Focusing for Circular Basis HyOPS Beams

The expression of HyOPS beams in paraxial optical fields, under circular polarization basis decomposition[24,29], can be written as,

$$\vec{E}(\rho,\theta) = E_0 e^{-\Gamma^2\rho^2}[B_1\rho^{|m|}e^{im\theta}\hat{e}_L + B_2\rho^{|n|}e^{in\theta}\hat{e}_R], \tag{1}$$

where $\hat{e}_L$ and $\hat{e}_R$ are left and right circular unit basis vectors respectively. In Eqn. 1, the integers m, n are the topological charges of the phase vortex beams with amplitude scaling factors B_1 and B_2 respectively, θ is azimuthal angle. E_0 is the amplitude of the beam, $\rho = \sin\phi/\sin\phi_{max}$ is the radial distance of a point from the center, normalized by the radius (a) of the lens. The truncation parameter is given by $\Gamma = a/w$, where w is the beam waist. It is a measure of the fraction of the beam inside the physical aperture of the lens. For a bright C-point either m or n is zero and $m \neq n$. So far, most studies concentrated on this type of beam[29,31]. Recently tight focusing of spatially varying optical fields embedded with polarization singularities such as bright C-points[46], dark C-points [25,47] and V-points[48] have been studied. The superposition described by Eqn. 1 can be realized by the Mach-Zehnder type interference, where the two arms carry the right circular and left circularly polarized beams, respectively.

Introducing the conic angle ϕ, the term $E_0 e^{-\Gamma^2\rho^2}$ in Eqn. 1 can be written as

$$E_0 e^{-\Gamma^2\rho^2} = E_0 e^{(-\Gamma^2\sin^2\phi/\sin^2\phi_{max})} = E_2(\phi), \tag{2}$$

where, ϕ is the focusing angle and ϕ_{max} is the maximum angle of convergence as depicted in Figure 1. The numerical aperture of an optical system is given by $NA = n_0\sin\phi_{max}$, where n_0 is the refractive index of the focal region. For an optical system shown in Figure 1, the electric field components in the focal region of an aberration-free aplanatic lens are given by [49,50]

$$\begin{aligned} E(u,v) = (-iA/\lambda)\int_0^{\phi_{max}}\int_0^{2\pi} E_2(\phi)P(\phi,\theta)A_2(\phi)\times e^{(ikW(\rho,\theta))} \\ \times e^{(-i\frac{v}{\sin\phi_{max}}\sin\phi\cos(\theta-\theta_P))}\times e^{(-i\frac{u}{\sin^2\phi_{max}}\cos\phi)}\sin\theta d\phi d\theta \end{aligned} \tag{3}$$

, where A is linked to the optical system parameters and λ is the wavelength of light in the medium with refractive index (n_0) in the focal region. In eqn.3, $W(\rho,\theta)$ corresponds to primary coma aberration. The primary coma aberration function is given by $W(\rho,\theta) = A_c\rho^3 cos\theta$ [27,28], where A_c is the comatic aberration coefficient in units of wavelength. $P(\phi,\theta)$ denotes polarization distribution at the exit pupil and $A_2(\phi)$ is the apodization factor. For an aplanatic lens system $A_2(\phi)$ is $\cos^{\frac{1}{2}}\phi$. The polarization distribution of the input field can be expressed as

$$P(\phi,\theta) = \begin{pmatrix} a_1(\cos\phi\cos^2\theta + \sin^2\theta) + b_1(\cos\phi\sin\theta\cos\theta - \sin\theta\cos\theta) \\ a_1(\cos\phi\sin\theta\cos\theta - \sin\theta\cos\theta) + b_1(\cos\phi\sin^2\theta + \cos^2\theta) \\ -a_1\sin\phi\cos\theta - b_1\sin\phi\sin\theta \end{pmatrix} \tag{4}$$

, where a_1 and b_1 are the strengths of the x and y components of the input field respectively. Optical coordinates at the observation plane or focal plane (x_Py_P-plane) are defined as

$$u = kz\sin^2\phi_{max}, \qquad v = k\sin\phi_{max}\sqrt{x_P^2 + y_P^2}, \tag{5}$$

where $k = 2\pi/\lambda$ is the propagation vector.

Preprints (www.preprints.org) | NOT PEER-REVIEWED | Posted: 22 December 2023 doi:10.20944/preprints202312.1701.v1

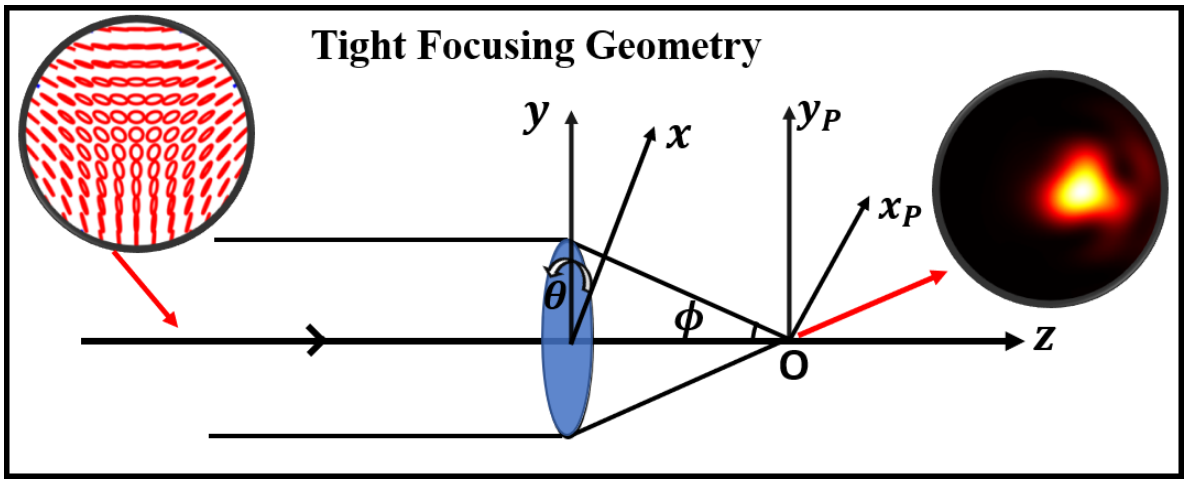

Figure 1. Geometric configuration for tight focusing of a right-handed bright star-type HyOPS beam in the presence of primary coma.

3. Intensity landscapes of circular basis HyOPS beams

Various parameters such as polarization distribution, total intensity distribution, and S_{12} Stokes field phase distribution of bright and dark generic HyOPS beams at the entrance pupil of the lens are numerically evaluated using Eqn. 1. Debye-Wolf integration (eqn. 3) is used to compute the focal plane transverse and longitudinal components of the input HyOPS beams for NA equal to 0.95. At the entrance pupil of the lens, the normalized Stokes parameters are computed by using transverse components of the HyOPS beams. Further, these normalized Stokes parameters are used to compute polarization parameters such as azimuth and ellipticity distributions. The azimuth and ellipticity distributions are used to demonstrate the polarization distributions of various HyOPS beams. Polarization, normalized intensity, and S_{12} Stokes field phase distributions of input HyOPS beams are depicted in row I of Figure 2 - Figure 7. The intensity distributions of the bright HyOPS beams, as shown in Figure 2 - Figure 4, at the entrance pupil of the lens corresponds to the Gaussian distribution. The intensity distributions of the dark HyOPS beams, as shown in Figure 5 - Figure 7, at the entrance pupil of the lens corresponds to the Laguerre-Gaussian (LG) distribution. In all the figures, Figure 2 - Figure 7, the focal plane intensity distributions of transverse (x and y) and longitudinal (z) components are depicted in row II, row III, and row IV respectively. In each case, the total intensity distribution is presented in row V. A HyOPS beam can be either left (h_L) or right (h_R) helicity [32,33]. For each HyOPS beam, the intensity and phase distributions corresponding to left and right helicity are shown in the left and right columns respectively. For an aberration-free optical system, the focal plane intensity and phase distributions corresponding to bright lemon and star-type HyOPS beams are depicted in Figure 2. In Figure 2, column I and column II correspond to the intensity distributions of left and right-handed lemon singularities respectively, and the corresponding component phase distributions are depicted in column III and column IV respectively. The right side of Figure 2 shows the intensity and phase distributions corresponding to bright left and right-handed star-type HyOPS beams. In a tight focusing system, a HyOPS beam and its index inverted field show completely different intensity distributions at the focal plane in terms of shape and symmetry. Even for the same polarization singularity index the focal plane intensity and phase distributions are found to be dependent on helicity and intensity of the HyOPS beams.

Preprints (www.preprints.org) | NOT PEER-REVIEWED | Posted: 22 December 2023 doi:10.20944/preprints202312.1701.v1

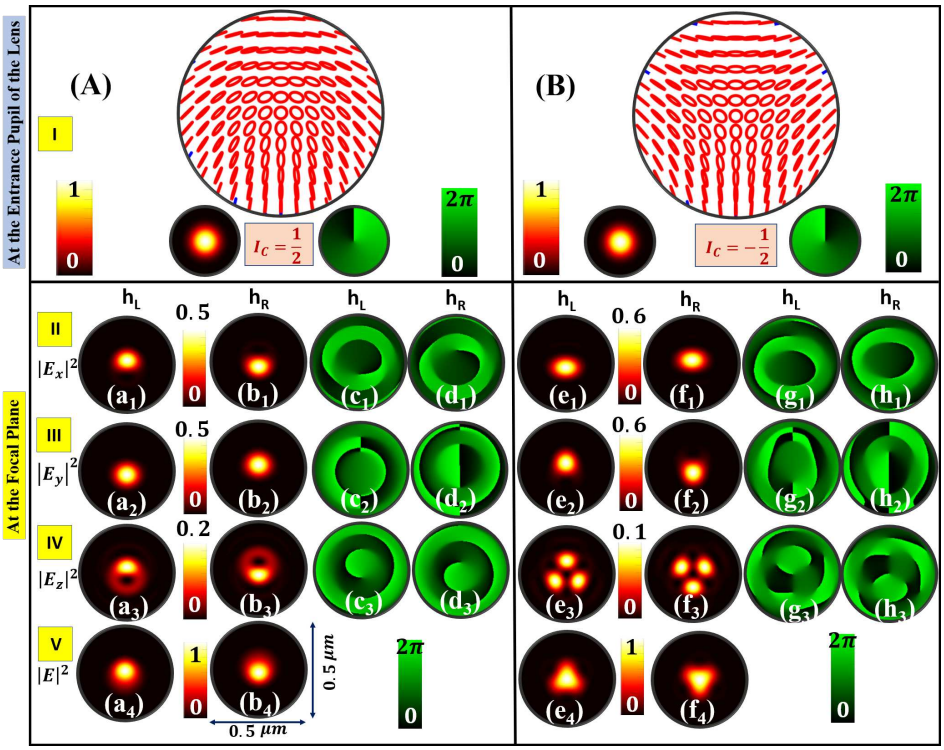

Figure 2. Bright HyOPS beams with (A) $I_C = \frac{1}{2}$; and (B) $I_C = \frac{-1}{2}$ are tightly focused. Focal plane component intensities are shown in row II ($|E_x|^2$), row III ($|E_y|^2$) and row IV ($|E_z|^2$) respectively. Normalized total intensity ($|E|^2$) distributions are shown in row V. Left and right helicity are denoted as h_L and h_R respectively. Phase distributions of the constituent field components are shown on the right side of the intensity distributions.

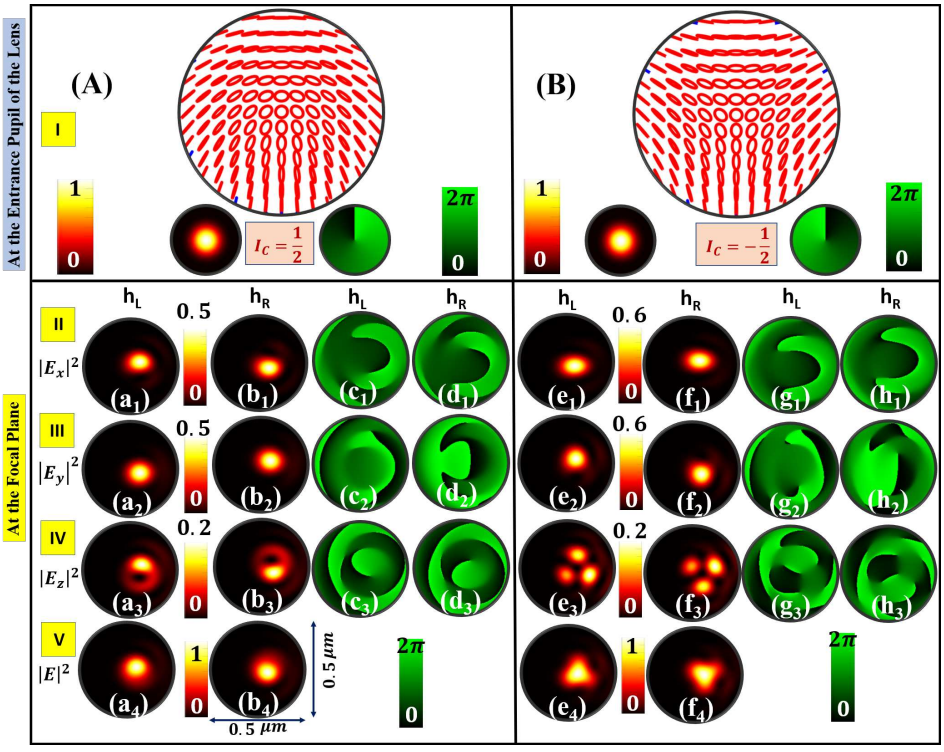

Figure 3. Bright HyOPS beams with (A) $I_C = \frac{1}{2}$; and (B) $I_C = \frac{-1}{2}$, as shown in Figure 2, are tightly focused in the presence of primary coma with primary coma strength $A_c = 0.50$.

Preprints (www.preprints.org) | NOT PEER-REVIEWED | Posted: 22 December 2023 doi:10.20944/preprints202312.1701.v1

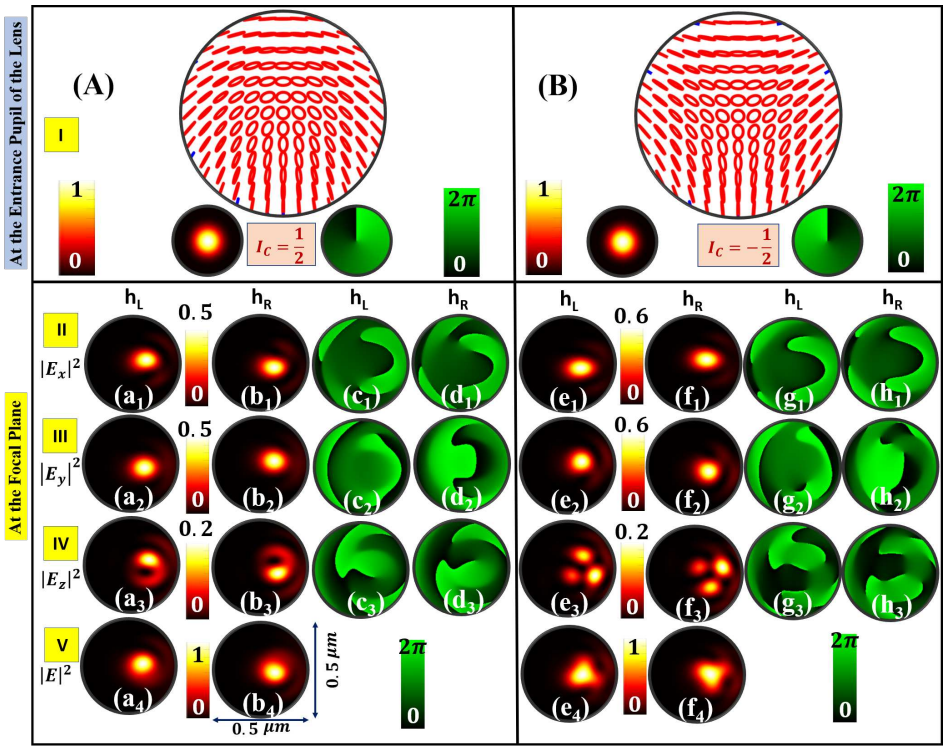

Figure 4. Bright HyOPS beams with (A) $I_C = \frac{1}{2}$; and (B) $I_C = \frac{-1}{2}$, as shown in Figure 2, are tightly focused in the presence of primary coma with primary coma strength $A_c = 0.75$.

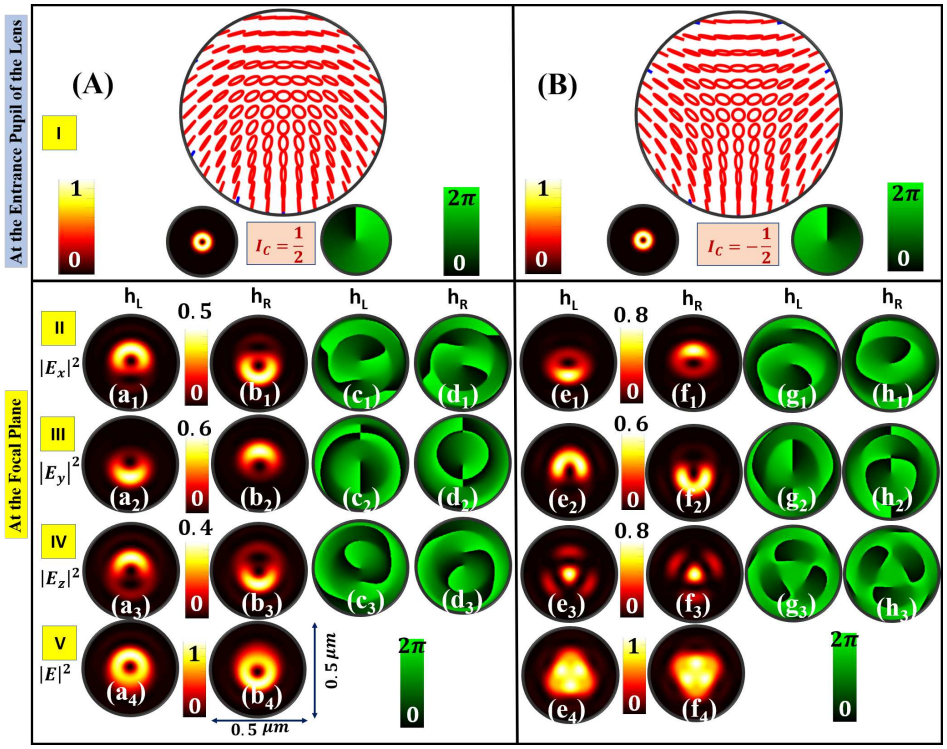

Figure 5. Dark HyOPS beams with (A) $I_C = \frac{1}{2}$; and (B) $I_C = \frac{-1}{2}$ are tightly focused. Focal plane component intensities are shown in row II ($|E_x|^2$), row III ($|E_y|^2$) and row IV ($|E_z|^2$) respectively. Normalized total intensity ($|E|^2$) distributions are shown in row V. Left and right helicity are denoted as h_L and h_R respectively. Phase distributions of the constituent field components are shown on the right side of the intensity distributions.

Preprints (www.preprints.org) | NOT PEER-REVIEWED | Posted: 22 December 2023 doi:10.20944/preprints202312.1701.v1

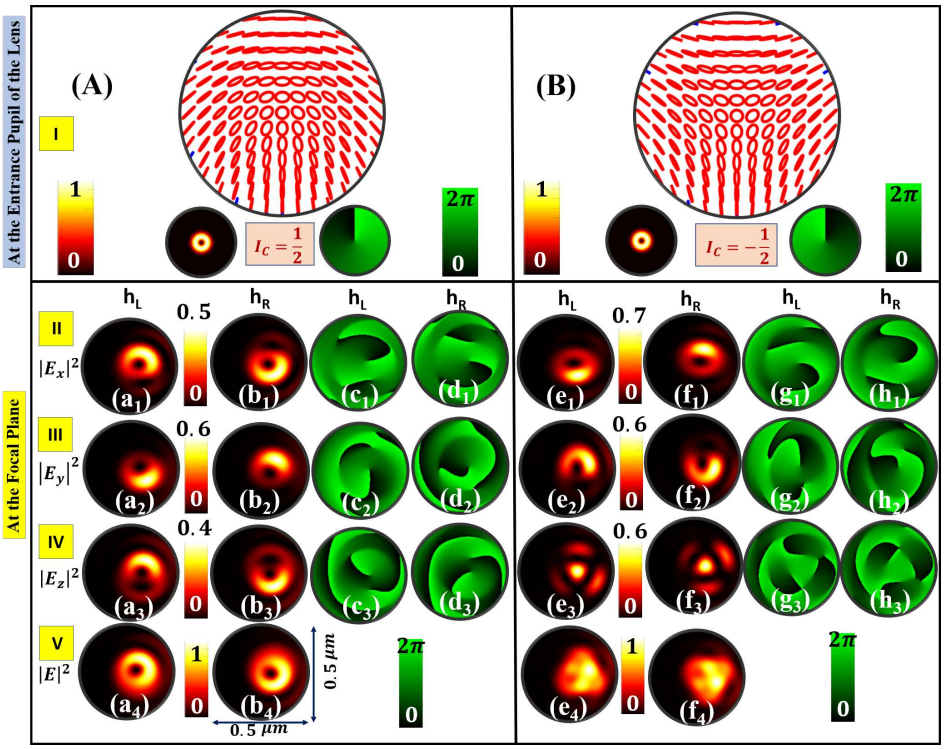

Figure 6. Dark HyOPS beams with (A) $I_C = \frac{1}{2}$; and (B) $I_C = \frac{-1}{2}$, as shown in Figure 5, are tightly focused in the presence of primary coma with primary coma strength $A_c = 0.50$.

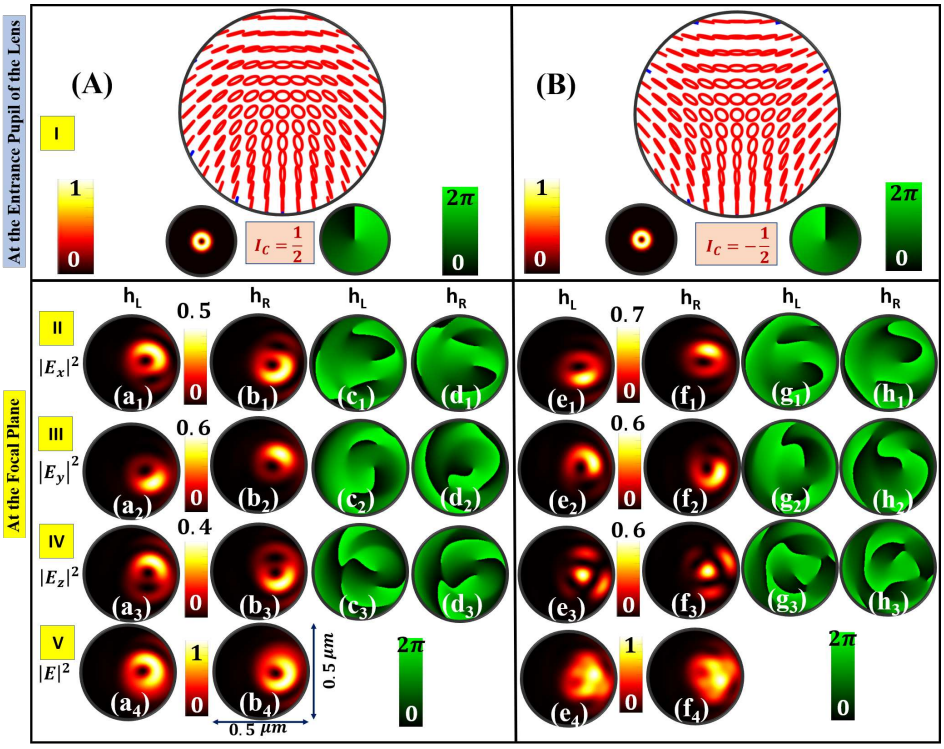

Figure 7. Dark HyOPS beams with (A) $I_C = \frac{1}{2}$; and (B) $I_C = \frac{-1}{2}$, as shown in Figure 5, are tightly focused in the presence of primary coma with primary coma strength $A_c = 0.75$.

Next, we study the effect of primary coma on the focal plane intensity and phase distributions for HyOPS beams as shown in Figure 2 for an optical system with NA 0.95. When the strength of the primary coma is $A_c = 0.50$, the focal plane intensity and phase distributions corresponding to

Preprints (www.preprints.org) | NOT PEER-REVIEWED | Posted: 22 December 2023 doi:10.20944/preprints202312.1701.v1

bright lemon and star-type HyOPS beams are shown in Figure 3. When the strength of the primary coma is $A_c = 0.75$, the focal plane intensity and phase distributions for bright lemon and star-type HyOPS beams are shown in Figure 4. From Figure 3 and Figure 4, it can be seen that the presence of primary coma in the optical system distorted the focal plane intensity distributions for both positive and negative index HyOPS beams. It is found that the presence of primary coma aberration in the focusing system produces a positional shift of the high-intensity lobes and a reduction of the intensity on one side of the center. As the strength of the primary coma increases, the focal plane intensity distributions shift more and more toward the right from the initial position. In the case of HyOPS beams, the focal plane intensity distribution undergoes rotation, as the helicity of the HyOPS beams is inverted, in addition to shifting in the presence of coma aberration. In all three cases, the focal plane field components are found to be embedded with phase vortices of charge ± 1. The appearance of phase vortices in the individual field components may be due to the superposition of polarization components of the electric field.

To generalize our study, we consider another class of HyOPS beams, known as dark HyOPS beams. First, we consider tight focusing of dark lemon and star-type HyOPS beams in the absence of primary coma, and the corresponding results are shown in Figure 5. Row I of Figure 5 depicts polarization, intensity, and S_{12} Stokes field phase distributions. In Figure 5, the focal plane intensity distributions corresponding to transverse (x and y component) and longitudinal (z-component) of the dark lemon and star-type HyOPS beams are shown in row II, row III, and row IV respectively. The total intensity distribution is presented in row V. In Figure 5, columns I and II correspond to focal plane component intensity distributions of left and right-handed dark lemon-type HyOPS beams respectively. The phase distribution corresponding to each component is depicted in columns III and IV respectively. The focal plane intensity and phase distributions of dark star-type HyOPS beams are shown in columns V to VIII. Similar to bright HyOPS beams, all three focal plane field components of the dark HyOPS beams are found to be embedded with phase vortices of charge ± 1. The effect of primary coma on the focal plane intensity and phase distributions of dark HyOPS beams for two different values of strength of primary coma are presented in Figs. 6-7. When the strength of the primary coma is $A_c = 0.50$, the focal plane intensity and phase distributions corresponding to dark lemon and star-type HyOPS beams are shown in Figure 6. Figure 7 shows the focal plane intensity and phase distributions for dark lemon and star-type HyOPS beams for $A_c = 0.75$. Similar to bright HyOPS beams, the presence of primary coma aberration is found to show a positional shift of the high-intensity lobes and a reduction of the intensity on one side of the center. As the strength of the primary coma increases, the focal plane intensity distributions shift more and more toward the right from the initial position. In addition to shifting the focal plane intensity and phase patterns also undergo helicity-dependent rotation in the case of tight focusing of HyOPS beams, which is not happening in the case of tight focusing of scalar vortices[27,28]. Note that in all the figures the focal plane component intensity distributions are normalized by the maximum value of the total intensity distribution.

4. Conclusions

In conclusion, we study the focal plane intensity and phase distributions of bright and dark circular basis HyOPS beams of $I_C = \pm\frac{1}{2}$ for a high numerical aperture (NA=0.95) system in the presence of a primary coma. It is shown that as the strength of the primary coma increases, the focal plane intensity as well as phase distributions shifted more and more toward the right from the initial position. The presence of primary coma aberration in the focusing system results in a positional shift of the high-intensity peaks, and a reduction of the intensity on one side of the center. For both positive and negative indexed bright and dark HyOPS beams, the focal plane intensity distribution undergoes rotation, as the helicity of the HyOPS beams is inverted, in addition to shifting.

Author Contributions: Conceptualization, Sushanta Kumar Pal; methodology, Sushanta Kumar Pal; formal analysis, Sushanta Kumar Pal, Rakesh Kumar Singh, P Senthilkumaran; investigation, Sushanta Kumar Pal,

P Senthilkumaran; data curation, Sushanta Kumar Pal; writing—original draft preparation, Sushanta Kumar Pal; writing—review and editing, Sushanta Kumar Pal, Rakesh Kumar Singh, P Senthilkumaran; visualization, Sushanta Kumar Pal; supervision, P Senthilkumaran; project administration, Sushanta Kumar Pal. All authors have read and agreed to the published version of the manuscript.

Funding: R. K. Singh acknowledges the Council of Scientific and Industrial Research, India, for a research grant $(80(0092)/20/EMR-II)$.

Institutional Review Board Statement: Not applicable

Informed Consent Statement: Not applicable

Data Availability Statement: The data that support the findings of this study are available from the corresponding author upon reasonable request.

Conflicts of Interest: The authors declare no conflict of interest.

Abbreviations

The following abbreviations are used in this manuscript:

HyOPS	hybrid order Poincaré sphere
HOPS	higher-order Poincaré sphere
SOP	State of polarization
NA	Numerical Aperture
PSF	point spread function

References

1. Linfoot, E.H.; Wolf, E. Diffraction Images in Systems with an Annular Aperture. *Proceedings of the Physical Society London B* **1953**, *66*, 145–149.
2. Welford, W.T. Use of Annular Apertures to Increase Focal Depth. *J. Opt. Soc. Am.* **1960**, *50*, 749–753.
3. Singh, K.; Dhillon, H.S. Diffraction of Partially Coherent Light by an Aberration-Free Annular Aperture. *J. Opt. Soc. Am.* **1969**, *59*, 395–401.
4. Slepian, D. Analytic Solution of Two Apodization Problems. *J. Opt. Soc. Am.* **1965**, *55*, 1110–1115.
5. Stamnes, J.J. Focusing of two-dimensional waves. *J. Opt. Soc. Am.* **1981**, *71*, 15–31.
6. Belland, P.; Crenn, J.P. Changes in the characteristics of a Gaussian beam weakly diffracted by a circular aperture. *Appl. Opt.* **1982**, *21*, 522–527.
7. Duan, K.; Lü, B. Nonparaxial analysis of far-field properties of Gaussian beams diffracted at a circular aperture. *Opt. Express* **2003**, *11*, 1474–1480.
8. Richards, B.; Wolf, E.; Gabor, D. Electromagnetic diffraction in optical systems, II. Structure of the image field in an aplanatic system. *Proceedings of the Royal Society of London. Series A. Mathematical and Physical Sciences* **1959**, *253*, 358–379.
9. Hao, B.; Burch, J.; Leger, J. Smallest flattop focus by polarization engineering. *Appl. Opt.* **2008**, *47*, 2931–2940.
10. Niziev, V.G.; Nesterov, A.V. Influence of beam polarization on laser cutting efficiency. *Journal of Physics D: Applied Physics* **1999**, *32*, 1455–1461.
11. Salamin, Y.I.; Keitel, C.H. Electron Acceleration by a Tightly Focused Laser Beam. *Phys. Rev. Lett.* **2002**, *88*, 095005.
12. Dorn, R.; Quabis, S.; Leuchs, G. Sharper Focus for a Radially Polarized Light Beam. *Phys. Rev. Lett.* **2003**, *91*, 233901.
13. Davidson, N.; Bokor, N. High-numerical-aperture focusing of radially polarized doughnut beams with a parabolic mirror and a flat diffractive lens. *Opt. Lett.* **2004**, *29*, 1318–1320.
14. Quabis, S.; Dorn, R.; Eberler, M.; Glöckl, O.; Leuchs, G. Focusing light to a tighter spot. *Optics Communications* **2000**, *179*, 1–7.
15. Ferrari, J.A.; Dultz, W.; Schmitzer, H.; Frins, E. Achromatic wavefront forming with space-variant polarizers: Application to phase singularities and light focusing. *Phys. Rev. A* **2007**, *76*, 053815.
16. Gupta, D.N.; Kant, N.; Kim, D.E.; Suk, H. Electron acceleration to GeV energy by a radially polarized laser. *Physics Letters A* **2007**, *368*, 402–407.

17. Youngworth, K.S.; Brown, T.G. Focusing of high numerical aperture cylindrical-vector beams. *Opt. Express* **2000**, *7*, 77–87.
18. Zhang, W.; Liu, S.; Li, P.; Jiao, X.; Zhao, J. Controlling the polarization singularities of the focused azimuthally polarized beams. *Opt. Express* **2013**, *21*, 974–983.
19. Schoonover, R.W.; Visser, T.D. Polarization singularities of focused, radially polarized fields. *Opt. Express* **2006**, *14*, 5733–5745.
20. Dennis, M.R. Fermionic out-of-plane structure of polarization singularities. *Opt. Lett.* **2011**, *36*, 3765–3767.
21. Freund, I. Cones, spirals, and Möbius strips, in elliptically polarized light. *Optics Communications* **2005**, *249*, 7–22.
22. Bauer, T.; Neugebauer, M.; Leuchs, G.; Banzer, P. Optical Polarization Möbius Strips and Points of Purely Transverse Spin Density. *Phys. Rev. Lett.* **2016**, *117*, 013601.
23. Bauer, T.; Banzer, P.; Bouchard, F.; Orlov, S.; Marrucci, L.; Santamato, E.; Boyd, R.W.; Karimi, E.; Leuchs, G. Multi-twist polarization ribbon topologies in highly-confined optical fields. *New Journal of Physics* **2019**, *21*, 053020.
24. Bauer, T.; Banzer, P.; Karimi, E.; Orlov, S.; Rubano, A.; Marrucci, L.; Santamato, E.; Boyd, R.W.; Leuchs, G. Observation of optical polarization Möbius strips. *Science* **2015**, *347*, 964–966.
25. Pal, S.K.; Somers, L.; Singh, R.K.; Senthilkumaran, P.; Arie, A. Focused polarization ellipse field singularities: interaction of spin-orbital angular momentum and the formation of optical Möbius strips. *Physica Scripta* **2023**, *98*, 055507.
26. Wang, Y.; Yong, K.; Chen, D.; Zhang, R. Influence of spherical aberration on the tightly focusing characteristics of vector vortex beams. *Opt. Express* **2023**, *31*, 28229–28240.
27. Singh, R.K.; Senthilkumaran, P.; Singh, K. Effect of primary coma on the focusing of a Laguerre–Gaussian beam by a high numerical aperture system; vectorial diffraction theory. *Journal of Optics A: Pure and Applied Optics* **2008**, *10*, 075008.
28. Singh, R.K.; Senthilkumaran, P.; Singh, K. Structure of a tightly focused vortex beam in the presence of primary coma. *Optics Communications* **2009**, *282*, 1501–1510.
29. Dennis, M.R. Polarization singularities in paraxial vector fields: morphology and statistics. *Opt. Commun.*, **2002**, *213*, 201–221.
30. Berry, M.V. The electric and magnetic polarization singularities of paraxial waves. *J. Opt. A: Pure Appl. Opt.* **2004**, *6*, 475–481.
31. Freund, I. Polarization singularity indices in Gaussian laser beams. *Opt. Commun.*, **2002**, *201*, 251 – 270.
32. Pal, S.K.; Senthilkumaran, P. Index polarity inversion by helicity inversion in Stokes vortices. *Applied Physics Letters* **2020**, *117*, 201101.
33. Pal, S.K.; Arora, G.; Ruchi.; Senthilkumaran, P. Handedness control in polarization lattice fields by using spiral phase filters. *Applied Physics Letters* **2021**, *119*, 221106.
34. Zhan, Q. Cylindrical vector beams: from mathematical concepts to applications. *Adv. Opt. Photon.* **2009**, *1*, 1–57.
35. Senthilkumaran, P. *Singularities in Physics and Engineering*; Number 2053-2563, IOP Publishing, 2018.
36. Yi, X.; Liu, Y.; Ling, X.; Zhou, X.; Ke, Y.; Luo, H.; Wen, S.; Fan, D. Hybrid-order Poincaré sphere. *Phys. Rev. A* **2015**, *91*, 023801.
37. Milione, G.; Sztul, H.I.; Nolan, D.A.; Alfano, R.R. Higher-Order Poincaré Sphere, Stokes Parameters, and the Angular Momentum of Light. *Phys. Rev. Lett.* **2011**, *107*, 053601.
38. Davis, J.A.; Nowak, M.D. Selective edge enhancement of images with an acousto-optic light modulator. *Appl. Opt.* **2002**, *41*, 4835–4839.
39. Samlan, C.T.; Suna, R.R.; Naik, D.N.; Viswanathan, N.K. Spin-orbit beams for optical chirality measurement. *Applied Physics Letters* **2018**, *112*, 031101.
40. Cipparrone, G.; Ricardez-Vargas, I.; Pagliusi, P.; Provenzano, C. Polarization gradient: exploring an original route for optical trapping and manipulation. *Opt. Express* **2010**, *18*, 6008–6013.
41. Pal, S.K.; Gangwar, K.K.; Senthilkumaran, P. Tailoring polarization singularity lattices by phase engineering of three-beam interference. *Optik* **2022**, *255*, 168680.
42. Pal, S.K.; Manisha.; Senthilkumaran, P. Phase engineering in overlapping lattices of polarization singularities. *J. Opt. Soc. Am. B* **2023**, *40*, 1830–1836.

43. Meier, M.; Romano, V.; Feurer, T. Material processing with pulsed radially and azimuthally polarized laser radiation. *Appl. Phys. A* **2007**, *86*, 329–334.
44. Shen, Y.; Martínez, E.C.; Rosales-Guzmán, C. Generation of Optical Skyrmions with Tunable Topological Textures. *ACS Photonics* **2022**, *9*, 296–303.
45. Xu, L.; Zhang, Y.; Lang, S.; Wang, H.; Hu, H.; Wang, J.; Gong, Y. Structured Illumination Microscopy Based on Asymmetric Three-beam Interference. *J. Innov. Opt. Health Sci.* **2021**, *14*, 2050027.
46. Pal, S.K.; Singh, R.K.; Senthilkumaran, P. Focal intensity landscapes of tightly focused spatially varying bright ellipse fields. *Journal of Optics* **2022**, *24*, 044013.
47. Pal, S.K. Tight focusing of orthogonal C-point polarization states. *Optik* **2023**, *274*, 170535.
48. Otte, E.; Tekce, K.; Lamping, S.; Ravoo, B.J.; Denz, C. Polarization nano-tomography of tightly focused light landscapes by self-assembled monolayers. *Nat. Commun.* **2019**, *10*, 4308.
49. Richards, B.; Wolf, E. Electromagnetic diffraction in optical systems, II. Structure of the image field in an aplanatic system. *Proceedings of the Royal Society of London A: Mathematical, Physical and Engineering Sciences* **1959**, *253*, 358–379.
50. Singh, R.K.; Senthilkumaran, P.; Singh, K. Effect of primary spherical aberration on high-numerical-aperture focusing of a Laguerre-Gaussian beam. *J. Opt. Soc. Am. A* **2008**, *25*, 1307–1318.